

Observations of Asian air pollution in the free troposphere at Mount Bachelor Observatory during the spring of 2004

Peter Weiss-Penzias,¹ Daniel A. Jaffe,¹ Philip Swartzendruber,^{1,2} James B. Dennison,^{1,3} Duli Chand,¹ William Hafner,¹ and Eric Prestbo⁴

Received 21 July 2005; revised 7 December 2005; accepted 13 February 2006; published 24 May 2006.

[1] This paper describes the chemical, aerosol, and meteorological measurements taken at Mount Bachelor Observatory (MBO), a new mountaintop site in central Oregon, USA (44.0°N, 121.7°W, 2763 m above mean sea level). During the initial campaign (28 March to 19 May 2004) we evaluated the utility of this location as a site to observe the global atmosphere, especially the free troposphere (FT). We observed some boundary layer (BL)/upslope flow during the daytime, which produced a 37–62% higher average water vapor mixing ratio (WV) compared to radiosonde data taken from similar altitudes in western Oregon. However, recently subsided air masses with low WV contained significantly elevated concentrations of carbon monoxide (CO), total gaseous mercury (TGM), and ozone (O₃), (25 ppbv, 0.16 ng/m³, and 13.9 ppbv, respectively), compared to periods with high-WV measurements. These enhancements represent a significant influence from Asian long-range transport (ALRT). One specific time period (“event”) on 25 April produced some of the largest CO, TGM, O₃, and particulate scattering (σ_{sp}) measurements ever seen along the West Coast due to ALRT. Enhancement ratios between these species are consistent with the major source being Asian industrial emissions. In particular, the Δ TGM/ Δ CO enhancement ratio was 0.0045–0.0048 ng/m³/ppbv for all ALRT events, similar to the value previously obtained from pollution plumes directly downwind of east Asia. A smaller pollution event of North American origin produced a Δ TGM/ Δ CO value of only 0.0013 ng/m³/ppbv, suggesting that the Δ TGM/ Δ CO value is an effective tracer of ALRT. Finally, thousands of kinematic back trajectories were calculated for each event to evaluate sources and transport processes.

Citation: Weiss-Penzias, P., D. A. Jaffe, P. Swartzendruber, J. B. Dennison, D. Chand, W. Hafner, and E. Prestbo (2006), Observations of Asian air pollution in the free troposphere at Mount Bachelor Observatory during the spring of 2004, *J. Geophys. Res.*, *111*, D10304, doi:10.1029/2005JD006522.

1. Introduction

[2] Research from the last few decades has shown that intercontinental transport of gaseous and particulate pollutants from Asia has a measurable impact on the atmospheric composition along the west coast of North America [e.g., Andreae et al., 1988; Parrish et al., 1992, 2004a; Jaffe et al., 1999, 2003a; Kotchenruther et al., 2001; Price et al., 2003; Weiss-Penzias et al., 2004]. With rising economic output in China and the east Asian region, industrial emissions have been increasing, along with emissions associated with land clearing and agriculture (fires and dust) [Horowitz and Jacob, 1999; Streets et al., 2003; Akimoto,

2003; Suntharalingam et al., 2004]. This appears to be at least partly responsible for the observed increase in background ozone (O₃) concentrations (6 ppbv since 1985) over western North America [Jaffe et al., 2003b; Parrish et al., 2004b]. Jacob et al. [1999] projected that if Asian anthropogenic NO_x emissions triple between 1985 and 2010, an increase of 2–6 ppbv of ozone is likely over the entire western United States, leading to difficulty for many urban regions to attain regional air quality objectives [Fiore et al., 2002].

[3] The majority of Asian long-range transport (ALRT) to North America occurs episodically during the spring [Yienger, 2000], because of lifting ahead of cold fronts on warm conveyor belts (WCBs) [Bey et al., 2001; Liu et al., 2003; Cooper et al., 2004a]. Deep cumulus convection has also been shown to be an important mechanism of vertical transport during the late spring [Oshima et al., 2004]. Once in the free troposphere (FT), pollutants can be transported in the midlatitude westerlies to the NE Pacific in 5–10 days [Price et al., 2004], where subsidence through anticyclones can then bring the pollutants down to the lower troposphere (<3 km) [Jaffe et al., 2003c; Hudman et al., 2004].

¹Interdisciplinary Arts and Sciences Department, University of Washington, Bothell, Washington, USA.

²Also at Atmospheric Sciences Department, University of Washington, Seattle, Washington, USA.

³Now at Washington State Department of Ecology, Olympia, Washington, USA.

⁴Frontier Geosciences, Seattle, Washington, USA.

Springtime aircraft observations during the PHOBEA [Kotchenruther *et al.*, 2001; Price *et al.*, 2003; Bertschi *et al.*, 2004] and the ITCT-2K2 [Nowak *et al.*, 2004; de Gouw *et al.*, 2004] campaigns have revealed relatively confined plumes of pollution and dust, which are attributable to Asian sources. Modeling studies have been successful in quantifying the carbon monoxide (CO) contribution from each source region [Jaeglé *et al.*, 2003; Liang *et al.*, 2004; Forster *et al.*, 2004], the primary tracer for ALRT, and suggest that about 1/3 of the springtime burden over the NE Pacific is of Asian industrial and biomass burning origin [Liang *et al.*, 2004]. Ozone has proven more difficult to simulate [Jaeglé *et al.*, 2003] because of its more complicated chemistry and stratospheric sources [Cooper *et al.*, 2004b].

[4] Airborne mercury (Hg), consisting of elemental (Hg^0), reactive (RGM), and particulate (PHg) is present in Asian industrial outflow, as determined from recent measurements at Okinawa, Japan [Jaffe *et al.*, 2005], and over the South China Sea [Friedli *et al.*, 2004]. Mercury is an air pollutant of great concern because of its high toxicity and its ability to bioaccumulate in the environment. The atmosphere has been identified as the most important cycling pathway in the global distribution of mercury because of the 6 month – 2 year estimated lifetime of Hg^0 [Schroeder and Munthie, 1998; Lin and Pehkonen, 1999]. Additionally, because of the large amounts of coal burned in east Asia presently [Wang *et al.*, 2000] and projected into the future, industrial Hg emissions from east Asia contribute about one half of the global anthropogenic total and are likely still increasing [Pacyna and Pacyna, 2002].

[5] Previous measurements of mercury species on the U.S. west coast at Cheeka Peak, Washington, in the marine boundary layer (BL) revealed little or no enhancements and weak correlations between Hg^0 and CO [Weiss-Penzias *et al.*, 2003]. However, our preliminary results as reported by Jaffe *et al.* [2005] identified a large mercury enhancement at Mount Bachelor Observatory (MBO) on one occasion during the spring of 2004 due to ALRT.

[6] Mountain-top free tropospheric observation sites are sparsely located across the northern hemisphere, and can provide unique information about the global atmosphere compared to sites in the BL [e.g., Bodhaine, 1996; Weingartner *et al.*, 1999]. The key questions that will be addressed here are the following: (1) How often and under what conditions is MBO sampling in the FT? (2) How can these air masses be distinguished from North American BL-influenced air masses? (3) What are the chemical signatures (enhancement ratios) that characterize long-range transport from Asia?

2. Methodology

2.1. Site Description and Sampling

[7] Mount Bachelor Observatory (MBO) is located atop a dormant volcano in the Cascade Range of central Oregon, USA (43.98°N 121.69°, 2763 m above sea level (ASL), see Figure 1). A ski area at the mountain operates from mid-November until the end of May, with most of the ski runs, lodges, access roads, and parking lots located on the eastern side of the mountain. Access to the summit is only via an electric-powered ski lift, hiking, or snow vehicle, with the

latter occurring ~once per day, and producing easily observable spikes in nitrogen oxides.

[8] The sampling site is located on the roof of the summit building and the instrument room is about 15-m below. The roof structure receives ice and snow buildup during stormy periods, which can persist for several days continuously. The roof is manually cleared of ice, but not on a regular basis. For this reason during this initial campaign, our sampling lines were located on the upper part of the leeward (SE) wall. This relatively protected location had to be cleared of ice only a few times during the spring.

[9] Carbon monoxide, ozone, and nitrogen oxides were sampled through 1/4" Teflon tubing, with a Teflon 1 μm particle filter at the inlet, which was changed bimonthly. The flow through this sample line was about 3 LPM, with the flow being shared about equally between the three instruments. Submicron particles were sampled through 3/8" copper tubing with no sharp bends to minimize particle loss in the tube and the inlet tip was fitted with a snow shield. The mercury sampling method is described in its own section below.

2.2. Meteorological Observations

[10] Temperature and relative humidity (T/RH) sensors (Campbell Scientific HMP 45C) were located at a lower height on the leeward wall of the building because they are less durable and could not withstand the heavy accumulation of ice that occurred on the very top of the building. Even at this more protected location, the T/RH housing collected ice on it during stormy periods ($T_{\text{amb}} < 0^\circ\text{C}$). Thus RH measurements $> 90\%$ for more than 24 hours continuously and with $T_{\text{amb}} < 0^\circ\text{C}$ were discarded from the data set because of probable RH sensor icing conditions. The total number of hours removed is 300 out of 1272.

[11] Water vapor mixing ratio (WV) was calculated from ambient relative humidity, temperature, and pressure (Vaisala PTB101B pressure transmitter) using an empirical equation from Bolton [1980]. When RH measurements were impacted by icing conditions, no WV data are reported. In late 2004 we added a method to directly measure WV from the high-flow gas inlet (Licor 6262). This method avoids the ice buildup problem of the external RH sensor; however these newer data are not included in the present analysis.

[12] Wind speed was measured with a Taylor Scientific WS-3 Heated Rotor Anemometer, and wind direction with a Taylor Scientific WD-3 Heated Direction Vane. These sensors also experienced icing periods in extreme weather conditions despite substantial heating of 1200 W. We removed 229 out of 1272 total hours (18%) because of icing.

2.3. Chemical Measurements

2.3.1. Carbon Monoxide

[13] Carbon monoxide was measured with two separate instruments: a Trace Analytical reduction gas analyzer (RGA) (28 March to 22 April) and a Thermo Electron Corporation nondispersive infrared (NDIR) CO analyzer (24 April to 19 May). The reduction gas analyzer is a gas chromatographic method that separates CO from other reductive gases (mainly H_2) and then measures the fluorescence of elemental mercury, which is produced from the reaction of $\text{CO} + \text{HgO(s)}$. The RGA method has a lower

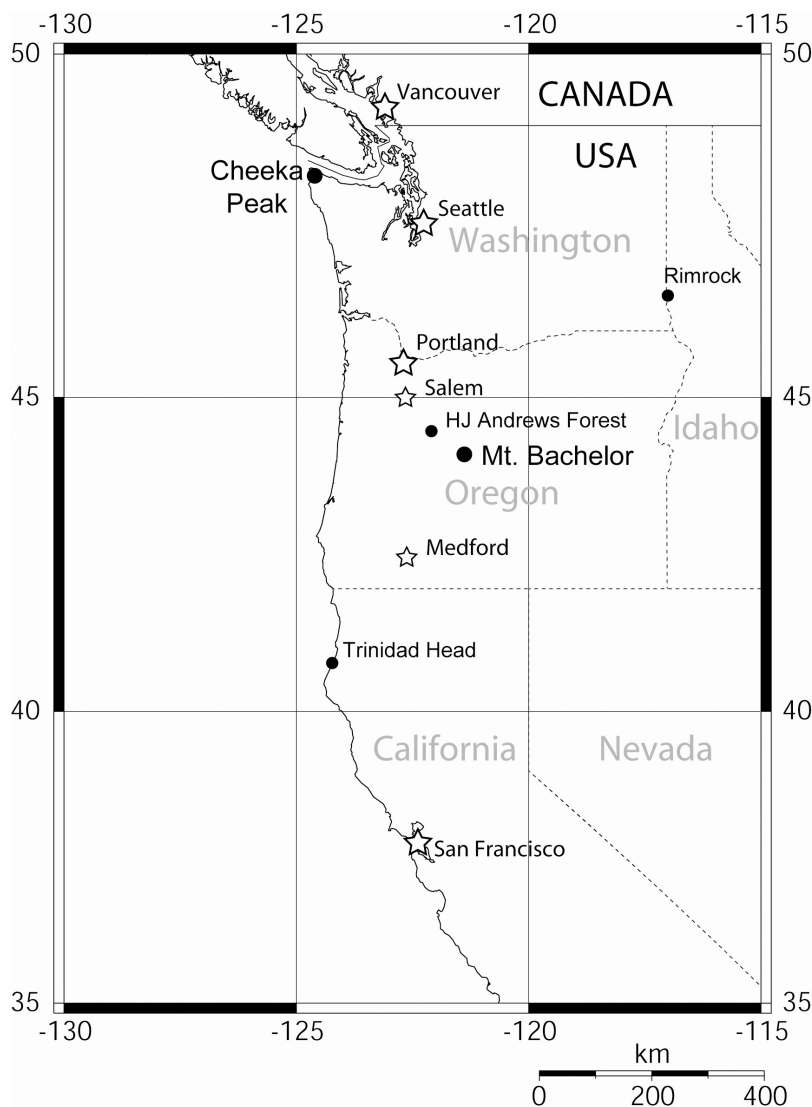


Figure 1. Map of the western United States, showing Mount Bachelor Observatory in relation to other key sites.

method detection limit (MDL) (10 ppbv) than the NDIR method (20 ppbv); however, the RGA was prone to temporary noise increases due to water contamination on the column. For this reason, the RGA is usually only used in our laboratory at the University of Washington, Bothell (UWB), to calibrate and cross-reference CO standards. The RGA made a single measurement every 4 min, whereas the NDIR makes continuous measurements with a response time of 1–2 min, resulting in about twice as much data taken per hour for the NDIR. Thus the total uncertainty in each hourly measurement from the RGA is about 12% and that from the NDIR is about 8%.

[14] Each instrument was calibrated at least daily with medical-grade breathing air containing a known amount of CO (429 ppbv), as determined both before and after the campaign in the laboratory using the RGA, referenced to a high-level NIST CO standard (9.75 ppmv, SRM# = 2612A) and an ambient-level CO cylinder (177 ppbv) from NOAA-CMDL [Novelli *et al.*, 1991]. We have employed this method of using breathing air for our CO standards and

analysis with the RGA against the NIST standard for several years and have found that the breathing air cylinders have minimal drift (<5%) over the period of field use (up to 6 months).

2.3.2. Ozone

[15] Ozone was measured using a standard UV absorbance instrument (Dasibi 1008 RS). This instrument was zeroed monthly using an activated charcoal scrubber cartridge and calibrated twice during the campaign with an ozone generator (Columbia Scientific Inc.), referenced to an ozone transfer standard from the Washington State Department of Ecology. The MDL is 1 ppbv and the estimated uncertainty in an hourly average is 2%.

2.3.3. Aerosol Scattering

[16] Submicron dry aerosol total scattering measurements (535 nm) (σ_{sp}) were made with a Radiance Research nephelometer. A 1 μm impactor was used at a flow rate of 10 LPM for the size cut. These values are expressed in $\text{m}^{-1} \times 10^6$, or Mm^{-1} corrected to STP (273K and 1 atm). The nephelometer was zeroed monthly using a high-effi-

Table 1. Mean Seasonal and Monthly Values ± 1 Standard Deviation for All Data^a

Dates	N, hours	CO, ppbv	TGM, ng/m ³	O ₃ , ppbv	σ_{sp} , Mm ⁻¹	Ambient T, °C	RH, %	Pressure, hPa	Wind Speed, m/s	Water Vapor (Calc), g/kg
<i>All Data</i>										
28 March to 19 May	1272	167 \pm 23	1.77 \pm 0.12	44.5 \pm 7.6	6.9 \pm 7.1	-1.5 \pm 5.1	60 \pm 23	729.2 \pm 5.3	10.1 \pm 6.0	3.2 \pm 1.0
28 March to 30 April	816	178 \pm 18	1.80 \pm 0.12	46.3 \pm 7.1	7.6 \pm 7.9	-2.0 \pm 5.4	56 \pm 24	729.2 \pm 5.8	9.8 \pm 6.3	2.9 \pm 0.9
1–19 May	456	147 \pm 15	1.70 \pm 0.08	41.8 \pm 7.5	5.7 \pm 5.4	-0.6 \pm 4.1	68 \pm 19	729.2 \pm 4.2	10.6 \pm 5.3	3.8 \pm 0.8
<i>Dry Data</i>										
28 March to 19 May	183	179 \pm 28	1.84 \pm 0.16	54.0 \pm 8.0	7.7 \pm 12	-2.3 \pm 5.7	43 \pm 26	731.6 \pm 3.7	10.6 \pm 6.9	1.7 \pm 0.5
<i>Wet Data</i>										
28 March to 19 May	183	154 \pm 22	1.69 \pm 0.08	40.0 \pm 5.4	7.3 \pm 4.6	2.5 \pm 2.7	74 \pm 13	730.6 \pm 3.7	9.5 \pm 6.2	4.6 \pm 0.3
<i>Dry – Wet</i>										
28 March to 19 May		+25	+0.16	+13.9	+0.4	-4.8	-31	+1.0	+1.1	-2.9

^aWater vapor segregated data for the whole season termed “dry” and “wet” is also shown along with dry – wet. Statistically significant ($P > 95\%$) differences are shown in bold.

ciency particle filter, and was calibrated with pure CO₂. The sample was heated so that RH < 35% before entering the nephelometer. The MDL for σ_{sp} is 0.25 Mm⁻¹ with an estimated hourly uncertainty of 5%.

2.3.4. Nitrogen Oxides

[17] Total reactive nitrogen oxides (NO_y), were measured with a standard chemiluminescence NO detector (Teledyne-API, model 200AU, MDL = 0.1 ppbv). These data were used only to detect the influence of snow grooming activities at the ski area, which were easily recognizable as large spikes, up to 10 ppbv. The rest of the periods, NO_y values were very low (mean = 0.16 ppbv) and displayed little correlation with other measurements.

2.3.5. Mercury

[18] The mercury measurements were made with a Tekran 2537A analyzer connected to a custom pyrolyzer and heated probe. We elected to add a pyrolyzer and heated probe in order to measure total gaseous (or airborne) mercury (TGM = Hg⁰ + RGM + PHg) rather than Hg⁰ because this method significantly reduces the potential for artifacts in the detection. Furthermore, we expect that the TGM signal will be dominated by Hg⁰ as in our previous measurements at Cheeka Peak, Washington [Weiss-Penzias *et al.*, 2003]. In our design, air was drawn through a quartz inlet which was held at about 130°C by a temperature controller. The probe was connected directly to a pyrolytic column composed of a quartz tube packed with quartz chips, which was maintained at 500°C in a tube furnace. The inlet system did not include any aerosol size segregation step so the upper particle size limit was limited by the efficiency of the inlet tip.

[19] The Tekran 2537A was configured to sample on a 5 minute collection cycle with a flow of 0.75 slpm, and had an MDL of 0.06 ng/m³. The instrument automatically calibrated to an internal permeation source every 18 hours. The accuracy of the factory determined permeation rate was compared to manual injections of a primary vapor source (Tekran 2505), and agreed to better than 6% with the factory specified rate. The hourly precision was 2% and the mean precision of successive internal calibrations was better than

1%. The overall uncertainty is estimated to be better than 16%. All mercury data are reported in ng per standard m³.

2.4. Supplementary Data

[20] Vertical profile data were incorporated into our analysis from two radiosonde sites: Medford, Oregon (42.4°N, 122.9°W, MFR), Salem, Oregon (44.9°N, 123.0°W, SLE), and one ozonesonde site: Trinidad Head, California (41.1°N, 124.2°W, THD) (see Figure 1 for locations). MFR and SLE meteorological data were obtained from the University of Wyoming (<http://weather.uwyo.edu/upperair/sounding.html>). THD ozonesonde data were obtained from NOAA-CMDL (<http://www.cmdl.noaa.gov/infodata/ftpdata.html> and B. Johnson, NOAA-CMDL, personal communications, 2004).

[21] Aerosol optical thickness (AOT) data were obtained from the NASA Aerosol Robotic Network (AERONET) for HJ Andrews Forest in Oregon and Rimrock in Idaho (<http://aeronet.gsfc.nasa.gov>).

2.5. Back Trajectories

[22] We calculated over 100,000 kinematic 10-day (241-hour) back trajectories from the Hybrid Single-Particle Lagrangian Integrated Trajectory (HYSPPLIT-4) model [Draxler and Rolph, 2003] (hereafter referred to as Hysplit trajectories). The Hysplit model was operated with meteorological input from the NCEP reanalysis data set which has a time resolution of 6 hours, a horizontal resolution of 2.5° latitude by 2.5° longitude, and 18 vertical layers. See section 3.7 for a discussion of this analysis.

3. Results and Discussion

3.1. Overview of Measurements

[23] Table 1 presents an overview (average $\pm 1\sigma$) of all measured parameters. This data set spans the time period 28 March to 19 May 2004 (“spring”), and is broken up into “April” and “May” sections (28 March to 30 April and 1–19 May). The measurements are also categorized into “dry” and “wet,” representing water vapor mixing ratio values

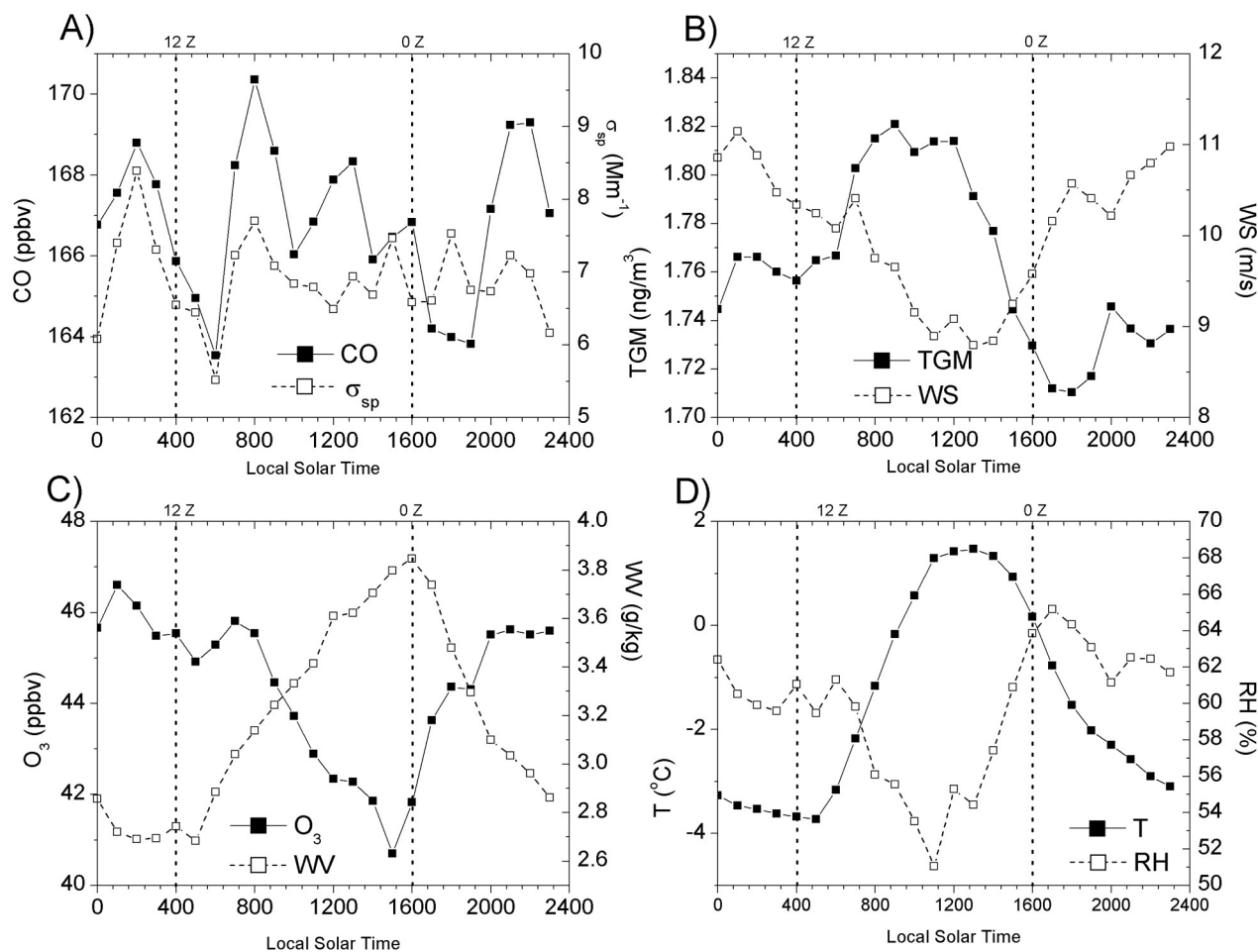


Figure 2. Average diurnal cycles for (a) CO and σ_{sp} , (b) TGM and WS, (c) O₃ and WV, and (d) T and RH from the spring 2004 campaign. In each plot the solid symbols belong to the left-hand axes and the open symbols belong to the right-hand axes. 0000 and 1200 UT times are shown which correspond to radiosonde launches in Figure 3.

less than 2.3 g/kg, and greater than 4.2 g/kg, respectively. The difference between “dry” and “wet” is also shown and discussed below.

[24] There is a distinct seasonal pattern in nearly all parameters, with concentrations of CO, TGM, O₃, and σ_{sp} being 21%, 6%, 10%, and 33% higher during April compared to May. WV on the other hand, is 31% lower in April. Standard deviations are higher in April across all parameters except for O₃. This seasonality is a function of (1) regional warming from April to May, which influences the relative amounts of FT and BL air seen at the site, (2) greater amounts of trans-Pacific transport in April [Liang *et al.*, 2004; Forster *et al.*, 2004], and (3) higher photolysis rates which leads to shorter lifetimes of CO, O₃, and TGM (species that react with hydroxyl radical (OH)) during May.

3.2. Diurnal Cycles

[25] In order to determine the degree to which daily changes in upslope/downslope flow on the mountain influenced our measurements, we calculated the average value for each parameter as a function of time of day during the spring campaign. Figure 2 shows the diurnal cycles of CO and σ_{sp} (Figure 2a), TGM and wind speed (WS) (Figure 2b),

O₃ and WV (Figure 2c), and T, and RH (Figure 2d), which are plotted against local time (LT). The variations as a fraction of the mean value for TGM, O₃, WV, WS, T, and RH are 7%, 12%, 34%, 22%, 2% (in Kelvin), and 11%, respectively. CO and σ_{sp} show no apparent diurnal pattern, which suggests that emission sources in the immediate region are not a significant influence on these measurements. O₃, WV, WS, T, and RH diurnal variations reflect some upslope/downslope mountain flow. Temperature reaches a maximum and WS and RH reach a minimum between 1100 and 1400 LT, during the time of highest zenith angle. The minimum in O₃ and the maximum in WV occur slightly later at 1500 and 1600 LT, respectively, and are a function of land heating bringing BL air upward to the summit. O₃ has a well known vertical gradient in the lowermost troposphere [Logan, 1999; Oltmans *et al.*, 2004] due to loss of O₃ to land/sea surfaces in the nocturnal boundary layer [e.g., Brown *et al.*, 2003], and less mixing from the upper troposphere. WV also displays a strong vertical gradient and thus these two parameters can be used to determine when predominantly FT or BL air is seen at MBO.

[26] Other mountain sites have observed much larger diurnal variability of gas and particle species than what we report here. For example, aerosol scattering measurements varied by a factor of 5 or more at Mauna Loa Observatory during the spring of 1992 [Bodhaine, 1996], which is probably due to more surface heating and a stronger upslope effect compared to MBO. Other measurements in the Swiss Alps have shown that deep alpine valleys are effective at vertically exporting pollutants to heights of at least 4 km during summer clear-sky conditions [Henne *et al.*, 2003]. Mt. Bachelor avoids this phenomenon somewhat, because it is almost a perfect cone-shaped mountain with very little glacially carved terrain, and thus air is not channeled up to the summit in alpine valleys. Thus, although MBO is not as high as other free tropospheric sites (e.g., Mauna Loa, 3.4 km; Jungfrauoch, 3.5 km), it will be shown that MBO can occasionally experience air that is representative of these higher altitudes.

[27] TGM shows a small diurnal variation of about 0.07 ng/m^3 about the mean, with a morning maximum (0800–1200 LT) and an evening/night minimum (1700–0400 LT). The maximum is shifted about 4–6 hours earlier than the WV maximum/ O_3 minimum cycle, suggesting that TGM is not simply controlled by BL-FT exchange due to daytime heating. Previous measurements have shown a similar phase in diurnal Hg^0 patterns (night/morning maximum, afternoon/evening minimum) [Lee *et al.*, 1998; Kellerhals *et al.*, 2003; Weiss-Penzias *et al.*, 2003; Poissant *et al.*, 2004]. Speciated Hg measurements (Hg^0 , RGM, and PHg), necessary to fully describe Hg dynamics, were begun during the spring of 2005 at MBO, and will be the subject of a forthcoming paper (P. Swartzendruber *et al.*, Observations of reactive gaseous mercury in the free troposphere at the Mt. Bachelor Observatory, submitted to *Journal of Geophysical Research*, 2006).

3.3. Altitude Comparison With Radiosonde Data

[28] In this section we present a comparison of the spring MBO data (including “dry” and “wet”) with the closest radiosonde sites at Medford (MFR) and Salem (SLE), Oregon, and an ozonesonde site at Trinidad Head, California (THD) (locations shown in Figure 1). It should be noted that each of these sites is in a different geographical region of the Pacific Northwest: MFR (400 m ASL) is in a valley between the Cascade and Coast mountain ranges, SLE (60 m ASL) is in the Willamette River valley, and THD (100 m ASL) is on the Pacific coast. Because of these geographical differences, the profiles differ somewhat. Figures 3a–3d show the vertical profiles of temperature (T), wind speed (WS), water vapor (WV), and ozone (O_3), compared to the MBO spring 2004, “day,” “night,” “dry,” and “wet” (see Figure 3 caption) at 729 hPa (2.8 km). MBO T and WS in Figures 3a and 3b are similar in magnitude to the vertical profiles at the same altitude. The diurnal variation of T is slightly greater than the range of values among the three vertical profiles at the same altitude. WS at MBO is slightly higher than the radiosonde data perhaps because of the summit itself, which could cause higher wind speeds because of ridge effects during occasional high-wind events. MBO WV is 37% and 62% higher than WV at 729 hPa from MFR and SLE, respectively, suggesting that MBO experiences more influence from the boundary layer compared to radiosonde data.

The offset between MBO and MFR in Figure 3c indicates that on average, MBO represents a somewhat lower altitude of 787 hPa (2.3 km) than the actual altitude of 729 hPa (2.8 km). This is consistent with our diurnal cycle findings (Figure 2) which show that there is regular mixing from lower altitudes, resulting in higher average WV mixing ratios.

[29] Average O_3 at MBO (44.5 ppbv) is significantly lower than the March–May 1997–2004 O_3 profile from Trinidad Head (57 ppbv) at 729 hPa, shown in Figure 3d. According to this comparison, the “equivalent altitude” of MBO is approximately 900 hPa (1330 m), much lower than that determined from the MFR WV comparison. However, this may not be an accurate comparison because THD is in a region of greater mean subsidence associated with the Pacific high. Modeled long-term vertical velocity values for April–May at 700 hPa are $+0.55 \text{ Pa/s}$ and -0.015 Pa/s for THD and MBO, respectively (available online at <http://www.cdc.noaa.gov>). In other words, THD at 729 hPa generally experiences air from higher altitudes because of greater regional subsidence compared to MBO, resulting in lower WV and higher O_3 .

[30] Thus, in order to generate a WV data set that is comparable to that from the same altitude over the MFR radiosonde site, we would retain 44% of the MBO data with $\text{WV} < 3.1 \text{ g/kg}$. Both data sets would then have a mean WV value of 2.3 g/kg . For the following analysis however, we will segregate the data by a more conservative WV cut-point of 2.3 g/kg , giving an average MBO WV value of 1.7 g/kg . This corresponds to the driest, subsiding air masses observed at MBO. In Figure 3c, comparing MBO “dry” with the MFR radiosonde data, gives an elevation for MBO of approximately 685 hPa (3.4 km). Average O_3 in these “dry” data (Figure 3d) also indicates that higher-altitude air masses are primarily being sampled. These data include 183 hours, which is 20% of the hours with valid WV data. These data are considered free tropospheric and are assumed to have had no contact with the North American continent in recent days. In contrast, we also examine the wettest 20% of the springtime data (“wet”), which correspond to all measurements with $\text{WV} > 4.2 \text{ g/kg}$. These data yield an “equivalent altitude” of 900 hPa (1330 m) according to Figure 3c, and are thought to be representative of the planetary boundary layer. Note that O_3 is significantly lower in these data as well (Figure 3d).

3.4. Comparison of Dry and Wet Segregated Measurements

[31] The “dry” and “wet” data sets differ considerably, which confirms our conceptual view of airflow at MBO; “dry” data represent air masses that have recently descended, have little influence from regional emissions, and may contain ALRT pollutants, and “wet” data have recently come from lower altitudes, may contain pollutants of North American origin, and may have been influenced by the clean marine boundary layer. Table 1 quantifies these differences. First, CO and TGM are significantly enhanced in the “dry” data because of the inclusion of several ALRT pollution plumes, higher background concentrations, and the natural seasonality of these two species (more hours in April). Second, ozone is also enhanced in the “dry” data, but in addition to ALRT, this may reflect the greater stratospheric influence in recently descended air. Additionally, O_3 in the “wet” data may have

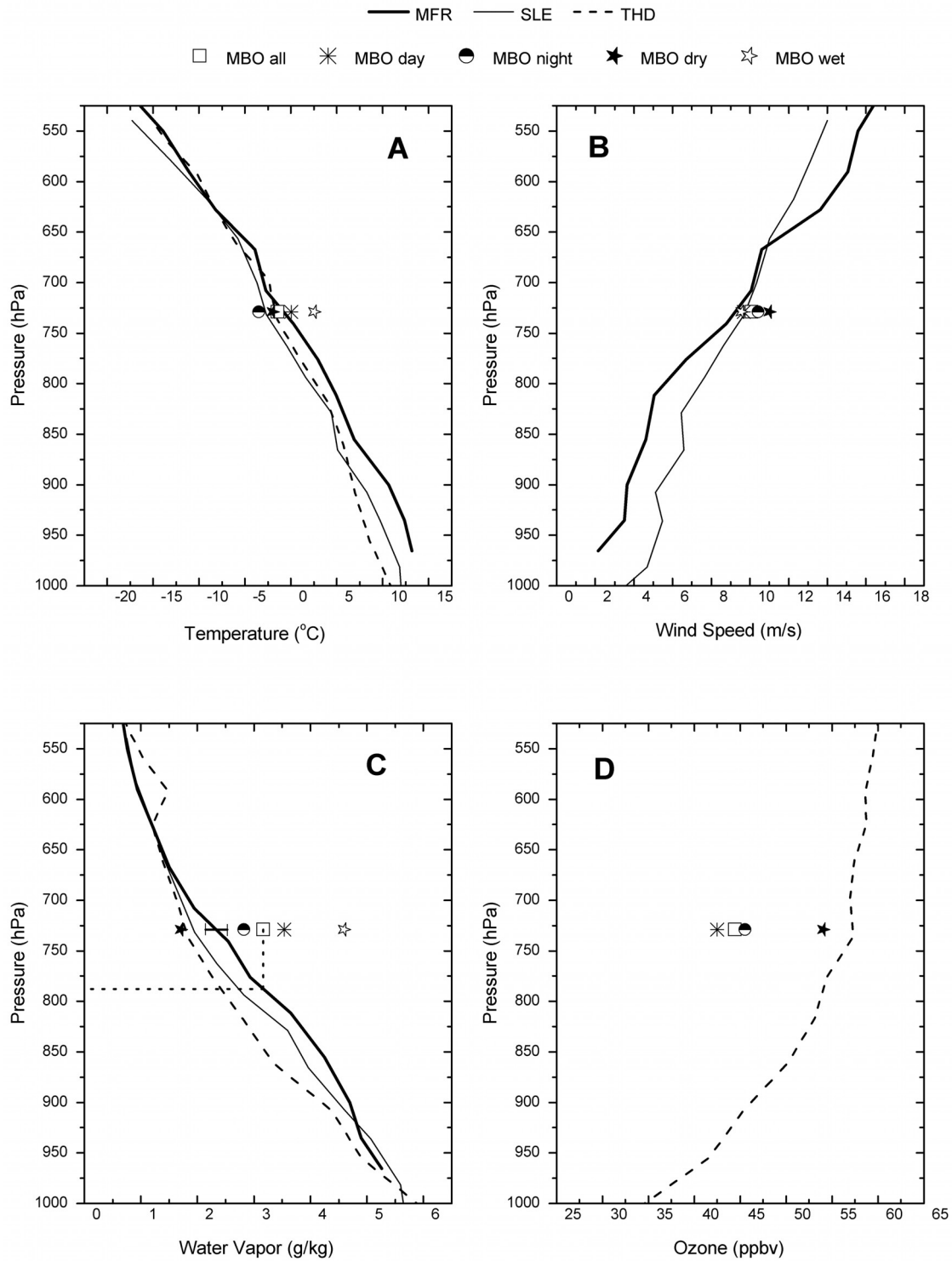


Figure 3. (a–d) Altitude comparison between the springtime 2004 MBO average at 729 hPa and vertical profiles from Medford, Oregon (MFR), Salem, Oregon (SLE), and Trinidad Head, California (THD). The MFR and SLE profiles represent an average from 0000 and 1200 UT, 28 March to 19 May 2004 ($n = 104$), while the THD profiles are the average from March to May 1997–2004 ($n = 110$). In each panel, diurnal variations at MBO are shown, where “day” = 1000–1400 LT and “night” = 2200–0200 LT. 0000 UT (right bar) and 1200 UT (left bar) variations are also shown for MFR in Figure 3c. “MBO dry” represents only those measurements when $WV < 2.3$ g/kg, and “MBO wet” represents $WV > 4.2$ g/kg. The dotted line in Figure 3c shows the approximate “equivalent altitude” of all MBO measurements in the spring.

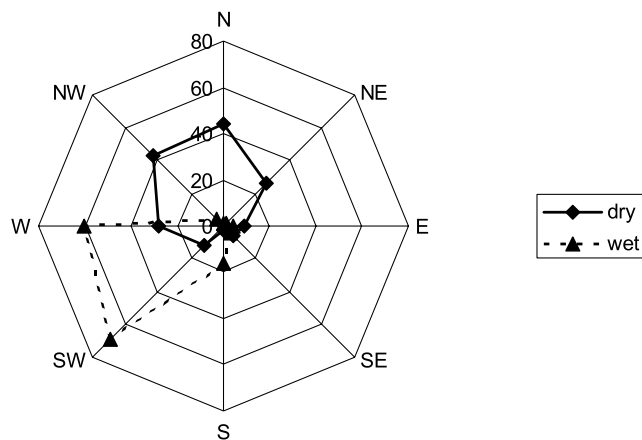


Figure 4. Wind direction distribution in number of hours per 45° sector for the “dry” and “wet” data sets.

been removed by surface deposition to the sea surface and vegetation. Third, σ_{sp} is not significantly enhanced in the “dry” data, which may reflect the shorter lifetime of σ_{sp} compared to CO and TGM. Also, local transport is probably more important for σ_{sp} than it is for CO and TGM. Fourth, “dry” air masses are considerably colder and have higher pressure, suggesting that these air masses are associated with anticyclonic flow. A comparison of wind direction distributions for the two data sets, shown in Figure 4, reveals that the prevailing wind direction during these “dry” periods is from the north, which confirms anticyclonic flow. “Wet” air masses have predominantly W and SW wind directions. Because of the sparse population in these directions, and close proximity to the Pacific Ocean (<300 km), the “wet” data do not show significant enhancements of CO or σ_{sp} . The strongest pollution events during the campaign (25 April and 13 May) were observed during dry subsiding air masses, and are attributed to distant pollution sources.

3.5. Comparison With Other Free Tropospheric Measurements in Pacific Region

[32] Table 2 compares CO, TGM, O₃, σ_{sp} , and WV measurements from MBO with past measurements in the

FT along the West Coast and across the Pacific. Also shown at the bottom of Table 2, are measurements from Cheeka Peak Observatory (CPO) in Washington State from 2002, a site at 500 m in the marine boundary layer, which is compared to our “wet” air measurements from MBO. Previous CO measurements from the PHOBEA campaigns show a relatively consistent mean value of about 140 ± 15 ppbv between 2 and 4 km, which is almost 40 ppbv lower than our “dry” CO value of 179 ± 28 ppbv. This significant jump in FT CO concentrations is consistent with recent observations from the MOPITT instruments [Shindell *et al.*, 2005] and NOAA-CMDL flask samples (P. Novelli, personal communication, 2005). Notice how TGM and σ_{sp} were also enhanced at MBO relative to past measurements, suggesting that higher levels of pollution transport occurred in 2004 compared to previous years. That this enhancement at MBO could be due to local sources is unlikely, since if this were the case, MBO “wet” data would show higher levels than MBO “dry” data. One explanation for the higher levels at MBO in 2004, then, is the large Siberian forest fires that occurred during the summer of 2003. Direct transport from these fires to the Pacific Northwest was observed [Jaffe *et al.*, 2004; Bertsch and Jaffe, 2005] and may have resulted in an increase in background CO concentrations persisting into the spring of 2004.

3.6. Pollution Transport Events: Chemical Data

[33] Three episodes of pollution transport are detailed in this section: two ALRT events on 25 April and 13 May, and one local pollution event on 27 April. The highest concentrations of CO, TGM, O₃, and σ_{sp} from the entire campaign occurred on 25 April. A close-up of this time period is shown in Figure 5a. Maximum hourly averages were 296 ppbv for CO, 2.52 ng/m³ for TGM, 78 ppbv for O₃, and 65 Mm⁻¹ for σ_{sp} , while WV was at a minimum of 1.8 g/kg. These pollutant concentrations are comparable to the largest plumes seen during ITCT-2K2 and PHOBEA aircraft campaigns [Nowak *et al.*, 2004; Price *et al.*, 2004]. In addition, this is the first documented TGM enhancement in a trans-Pacific ALRT plume. The peak of the event occurred at night during strong subsidence, enhanced pressure (max. = 737 hPa), low wind speeds (min. = 0.5 m/s), and a negative correlation between

Table 2. Comparison of All-Spring and WV-Segregated Data From MBO With Other Measurements in the 2–4 km Altitude Range Along the West Coast and Across the Pacific During the Spring^a

Location	Altitude, km	Dates	N	CO, ppbv	TGM, ng/m ³	Ozone, ppbv	σ_{sp} , Mm ⁻¹	WV, g/kg	Reference
MBO (dry)	2.7	28 March to 19 May 2004	183 hours	179	1.84	54.0	7.7	1.7	this work
PHOBEA '02, aircraft	2.5–3.5	29 March to 23 May 2002	13 flights	140	...	49	3.0	...	Bertschi <i>et al.</i> [2004]
PHOBEA '01, aircraft	2.5–3.5	29 March to 6 May 2001	12 flights	139	...	45	3.3	1.7	Price <i>et al.</i> [2003]
PHOBEA '99, aircraft	2–4	26 March to 28 April 1999	14 flights	139	...	60	4.8	2.0	Kotchenruther <i>et al.</i> [2001]
ACE-Asia, aircraft	2–3	31 March to 30 April 2001	16 flights	...	1.65	Friedli <i>et al.</i> [2004]
MBO (wet)	2.7	28 March to 19 May 2004	183 hours	154	1.69	40.0	7.3	4.6	this work
Cheeka Peak, Washington (marine and nonmarine)	0.5	28 March to 19 May 2002	1272 hours	147	1.42	43.3	3.8	5.1	Weiss-Penzias <i>et al.</i> [2003, 2004] and P. Weiss-Penzias, unpublished data, 2001

^aAlso shown are the measurements from Cheeka Peak, Washington, from 2002, a site in the marine boundary layer.

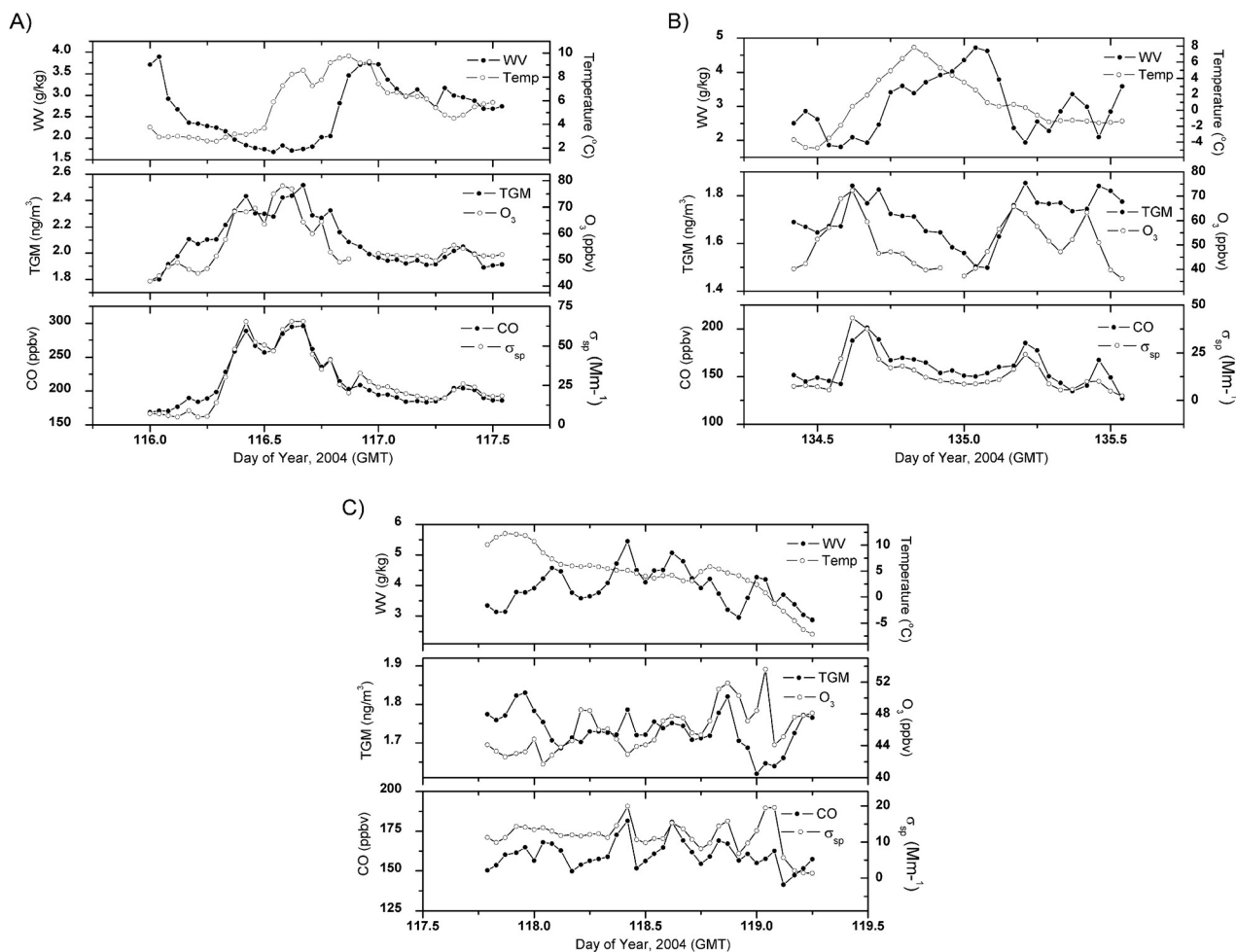


Figure 5. Measurements during the (a) 25 April, (b) 13 May, and (c) 27 April pollution events. In each plot the solid symbols belong with the left axes, and the open symbols belong with the right axes.

CO and WV ($r = -0.72$). Temperature climbed to 10°C during this event, which may have resulted in the thermal decomposition of PAN and enhanced O_3 formation [Hudman *et al.*, 2004].

[34] The 13 May event is shown in Figure 5b. This event is characterized by lower peak concentrations than the 25 April event: $\text{CO} = 200$ ppbv, $\text{TGM} = 1.87$ ng/m^3 , $\sigma_{\text{sp}} = 45$ Mm^{-1} , and $\text{O}_3 = 72$ ppbv. These lower concentrations are partially a result of less subsidence (maximum pressure = 731 hPa), yielding a weaker CO/WV correlation ($r = -0.53$).

[35] The 27 April event was the smallest of the three pollution episodes, shown in Figure 5c. CO, TGM, O_3 , and σ_{sp} have maxima at 180 ppbv, 1.8 ng/m^3 , 49 ppbv, and 20 Mm^{-1} , respectively, and in contrast to the 25 April and 13 May events, WV reaches a maximum of 5.5 g/kg. While these concentration enhancements are not great, this event displays a strong positive correlation between CO and WV ($r = 0.85$) and between CO and σ_{sp} ($r = 0.78$), suggesting that polluted air from the BL was observed. Meteorologically, this event was characterized by rapidly cooling temperatures (from 10 to 3°C), falling pressure (from 740 to 734 hPa), and increasing wind speeds (from 7 to 20 m/s). These conditions suggest a cold front was

approaching the site, quite different from high pressure subsidence observed for the other events. The main peak of the event occurred on 27 April at 1000 UT, and displays a small increase in TGM, and a loss in O_3 . The latter observation may be a result of loss of O_3 to deposition, if in fact the air masses had contact with the surface.

[36] Linear correlation coefficients and slopes for TGM/CO, O_3/CO , and $\sigma_{\text{sp}}/\text{CO}$ for each event are shown in Table 3. Differences between the ALRT and local events are evident in these data. The ALRT events are believed to be composed mainly of Asian industrial pollution with very little biomass burning or dust emissions. This conclusion is drawn by comparing the enhancement ratios (ERs) between species (i.e., the slopes of the linear correlations) with ERs obtained from previous measurements of Asian pollution. First, the TGM/CO ERs have been postulated to be sensitive indicators of ALRT because of the large mercury emissions in China; a value of 0.0056 ± 0.0016 $\text{ng}/\text{m}^3/\text{ppbv}$ is thought to be indicative of Asian industrial emissions [Jaffe *et al.*, 2005]. Indeed, this is the same ER that was observed by Friedli *et al.* [2004] in a plume downwind of Shanghai, China. Because of the long lifetimes of CO (1–6 months) and Hg^0 (6–24 months), we would expect to see this ER conserved during trans-Pacific ALRT. $\Delta\text{TGM}/\Delta\text{CO}$ from

Table 3. Correlation Coefficients and Slopes (Using Hourly Averages) for Two Long-Range Transport Events, 25 April and 13 May, and One Local Pollution Event, 27 April^a

Event	TGM/CO		O ₃ /CO		σ _{sp} /CO	
	R	Slope, ng/m ³ /ppbv	r	Slope, ppbv/ppbv	r	Slope, Mm ⁻¹ /ppbv
25 April 2004 (n = 29)	0.95	0.0045	0.89	0.22	0.97	0.47
13 May 2004 (n = 18)	0.72	0.0048	0.32	0.22	0.78	0.47
27 April 2004 (n = 18)	0.43	0.0013	-0.13	...	0.78	0.20

^aSlopes are only shown for r-values > |0.3|.

both the 25 April and 13 May events is in fact remarkably consistent at 0.0045–0.0048 ng/m³/ppbv. Second, the $\Delta\sigma_{sp}/\Delta\text{CO}$ values from both ALRT events (0.47 Mm⁻¹/ppbv) agree with the ERs from ALRT events (0.5 Mm⁻¹/ppbv) between 0 and 5 km observed during the PHOBEA campaigns [Price *et al.*, 2004]. Previous ALRT events containing large amounts of biomass burning emissions have resulted in $\Delta\sigma_{sp}/\Delta\text{CO}$ values that are about a factor of 2 larger than what we observe here [Bertschi *et al.*, 2004]. Third, the $\Delta\text{O}_3/\Delta\text{CO}$ value for both ALRT events is 0.22 ppbv/ppbv, which would be classified as “Type-II” according to Price *et al.* [2004], and falls within the 0.1–0.5 range that are typical ERs from industrial pollution.

[37] ERs from the 27 April local event are quite different from the ALRT events and are another way to distinguish between “dry” and “wet” air masses. In particular, the $\Delta\text{TGM}/\Delta\text{CO}$ value is considerably less (0.0013 ng/m³/ppbv) than the value that is attributed to Asian industrial pollution. A smaller value in local pollution is consistent with a lack of mercury sources in the region around MBO [Jaffe *et al.*, 2005]. O₃ also behaves quite differently in this local event, being uncorrelated with CO. This suggests a lack of photochemical production and/or loss to surface deposition. σ_{sp} is well correlated with CO in this event, but the $\Delta\sigma_{sp}/\Delta\text{CO}$ ratio is less than that observed during the ALRT events. This may have been caused by precipitation associated with the approaching cold front, which would remove particles but not CO and result in a lower ER.

3.7. Pollution Transport Events: Back Trajectory Analysis

[38] Kinematic back trajectories from Hysplit were used to verify source regions for the 25 April, 13 May, and 27 April pollution events. Our analysis is patterned after the work of Stohl *et al.* [2002, 2003], who introduced the term “retroplumes.” The idea is that thousands of trajectories must be calculated, each one representing the path of a single particle, in order to have a large enough sample size that can begin to represent air mass transport. These trajectories were used to calculate how many hours a particle of air had spent in a predefined “east Asian” box (20–45°N by 100–130°E by 0–10 km, see Figure 9), and we refer to those hours as “residence time” as a function of altitude in the box. The size and placement of the box roughly corresponds to the region of large CO concentrations as revealed from the MOPITT instrument (data available online at <http://www.eos.ucar.edu/mopitt/>). We calculate hourly trajectories whose start locations are every 100 m of altitude from 0 – 2900 m above ground level (AGL), and every 0.125° in a 0.5° latitude × 0.5° longitude box centered on MBO. This results in a total of 25 trajectories generated per hour for every 100 m of altitude. Hysplit calculates ground level in the grid square

containing MBO to be approximately 830 m above sea level, putting the actual summit of Mt. Bachelor at about 1940 m AGL.

[39] The results of these calculations are shown in Figure 6. Residence times in the east Asian box are given by different colors and line styles as a function of altitude in the east Asian box. From these plots we observe that there are peaks in residence times that roughly correspond to the 25 April and 13 May ALRT events. The peak on day 116 (25 April) is the largest of the whole time period confirming that the source of this large pollution event was within the east Asian box. The residence time calculations also show that the 13 May event was much smaller (note different y axis) and was composed of two peaks – a feature that shows up in our data (see Figure 5b). There is also agreement with the 27 April event in that there is a period where residence time in the east Asian box goes to zero just before 1200 UT.

[40] There is an interesting result in Figure 6 that points out the potential limitation of using trajectories for this type of analysis. Note that the residence times for trajectories <1 km in the box are very low and almost insignificant. Residence times for <2 km and <3 km show much more structure. This indicates that trajectories do not resolve BL-FT exchange processes in the east Asian box very well, which is probably a function of coarse wind field resolution, and trajectory errors associated with turbulent flow and convection [Stohl, 1998]. Thus we will focus on trajectory residence times <3 km in the east Asian box as representing air masses having been in contact with the source region.

[41] The peak in trajectory residence times for both ALRT events shown in Figure 6 is slightly offset (~12 hours early) compared to the maximum concentrations observed at MBO (compare to Figures 5a and 5b). Figure 7 shows that the agreement between trajectories and observations is much better when a starting altitude of about 1500 m AGL is used for MBO, instead of the 1900–2900 m AGL used in Figure 6. 1500 m AGL is approximately 440 m lower than the actual height of MBO and shows the importance of running trajectories at many altitudes in order to capture plumes that might be descending over time.

[42] Further evidence of the subsiding air mass on 25 April is given by total column aerosol optical thickness (AOT) measurements at 500 nm, taken at two sites in the Pacific Northwest, shown in Figure 8. Here we see that the peak in AOT occurred at approximately day 116.0, which corresponds to the peak in trajectory residence times between 2500 and 2900 m AGL in Figure 7. Thus, even though Rimrock, Idaho is to the east of MBO, a large part of the plume evidently passed over this location at higher altitudes before descending to MBO.

[43] Back trajectory diagrams showing long-range and local transport are shown in Figures 9–11 for the 25 April,

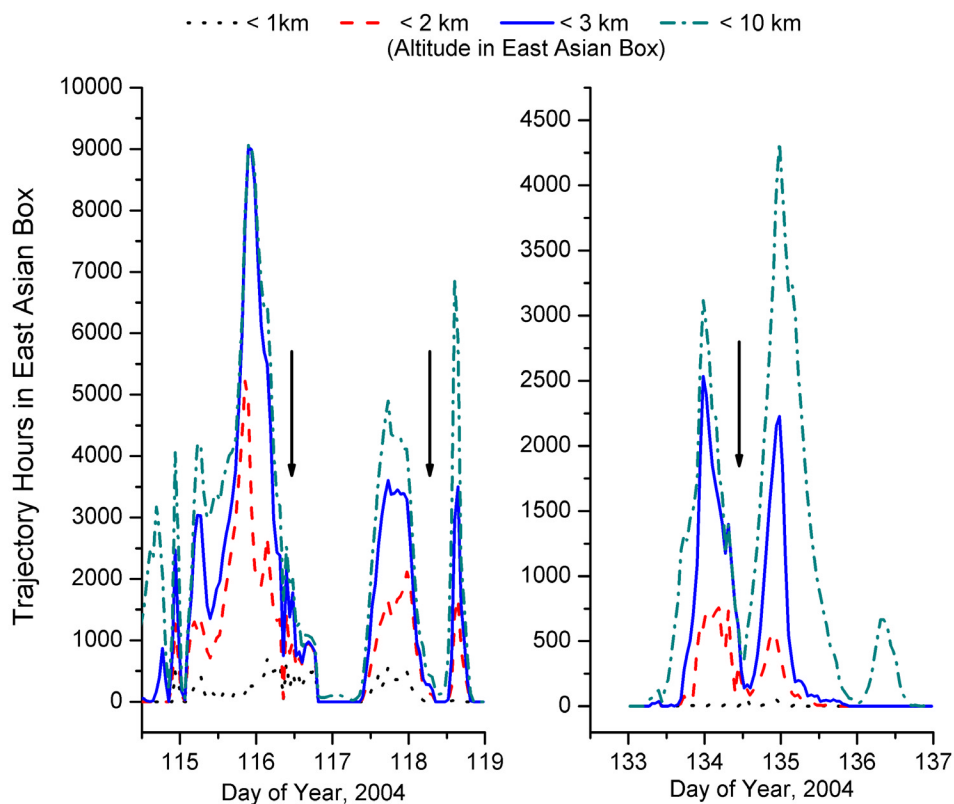


Figure 6. Residence times of back trajectories in the east Asian box, for various heights in the box (shown as different colors and line styles). Each line represents the sum of the residence times with starting heights at MBO every 100 m between 1900 and 2900 m AGL, calculated every hour for the time periods 23–28 April and 12–15 May. Arrows refer to the peaks in concentrations during the events at MBO.

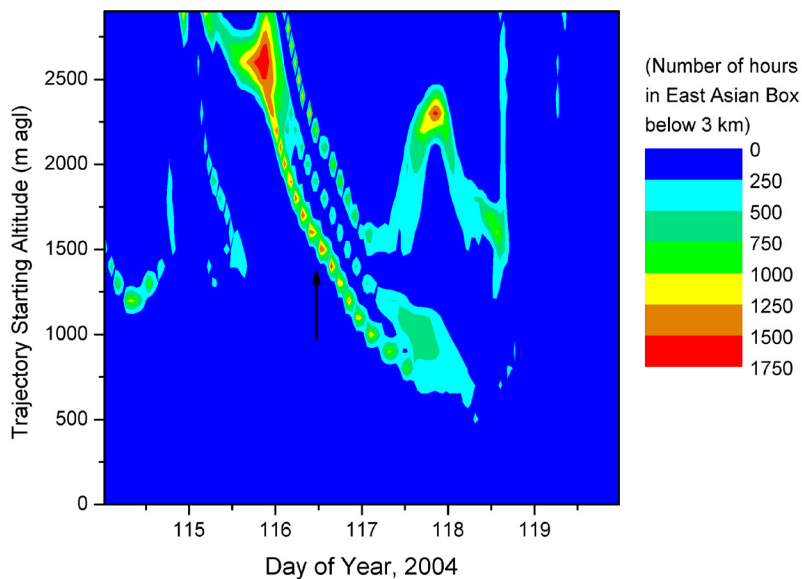


Figure 7. Residence times of back trajectories < 3 km in the east Asian box (color scale) as a function of time (x axis) and trajectory starting altitude at MBO (y axis). The black arrow indicates the approximate peak in observations during the 25 April event at MBO.

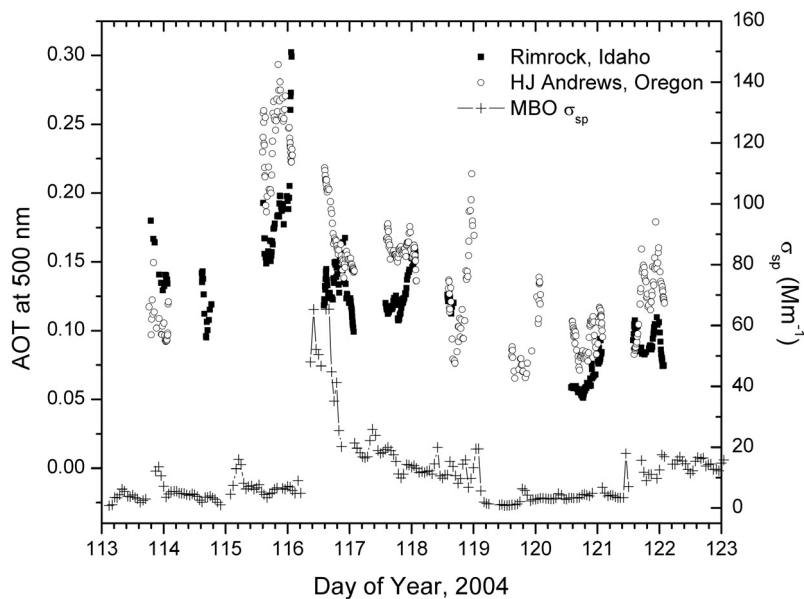


Figure 8. Total column aerosol optical thickness (AOT) at 500 nm from AERONET during the month of April 2004, measured at two locations in the Pacific Northwest region and compared to MBO aerosol scattering measurements.

13 May, and 27 April events, respectively. Figure 9 shows that for the 25 April event, air masses picked up pollutants from northeastern China, Korea and/or southern Japan about 9–10 days back. Then the air masses were lifted 5–7 days back into the midlatitude westerlies, indicated by trajectories at altitudes > 10 km. These high-altitude trajectories actually cross Europe 10 days back, indicating very fast transport. Finally, the trajectories show descending air masses to MBO starting about 1.5 days back.

[44] Figure 10 shows very tightly confined back trajectories for the 13 May event. The probable source region for this event is quite similar to that of the 25 April event and explains the relatively uniform interspecies ERs between

events (see Table 3). These trajectories also show considerable lifting of air masses between days 5–7 to altitudes > 10 km, which if stratospheric air were mixed in, could explain the weaker correlations with O₃ in this event. Once again, subsiding air masses are well represented by these trajectories between 0–3 days back.

[45] Figure 11 and its inset show transport over North America during days 0–2 for the 27 April event. From these trajectories it appears that the source of this weak pollution event was most likely western Oregon (Eugene or Medford), or perhaps northern California (Sacramento). High wind speeds and turbulent BL flow probably diluted this plume considerably. Figure 11 also shows that a few trajectories enter the east Asian box and thus might influence the pollutant concentrations somewhat. However, most

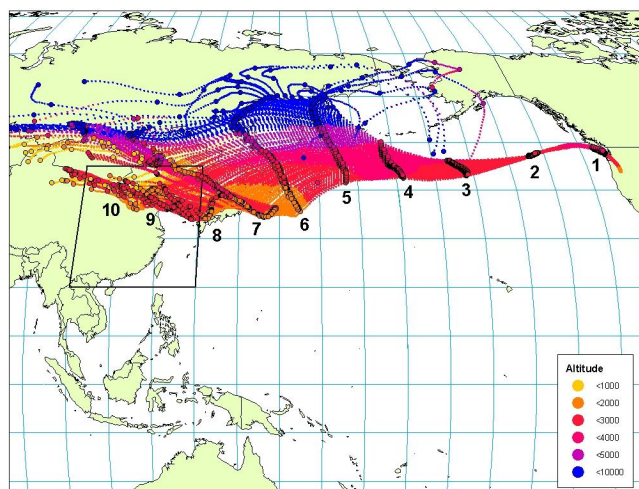


Figure 9. Back trajectory diagram with starting times of 25 April (1000–1600 UT) and a starting altitude of 1500 m AGL. A total of 175 trajectories are shown, and the numbers refer to the number of days backward in time from MBO.

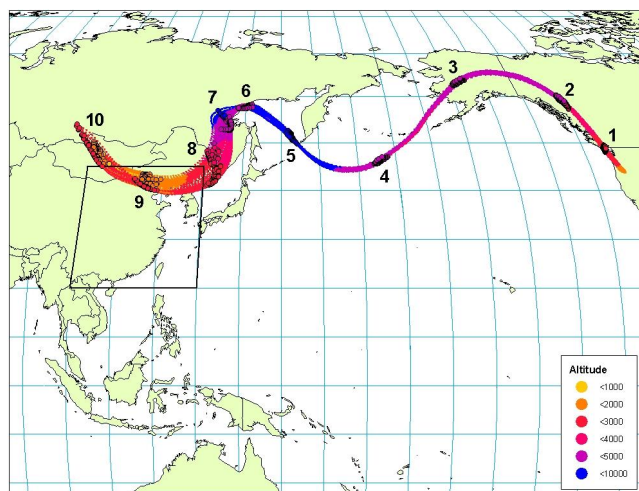


Figure 10. Back trajectory diagram with starting times of 13 May (1000–1400 UT) and a starting altitude of 1800 m AGL. A total of 125 trajectories are shown.

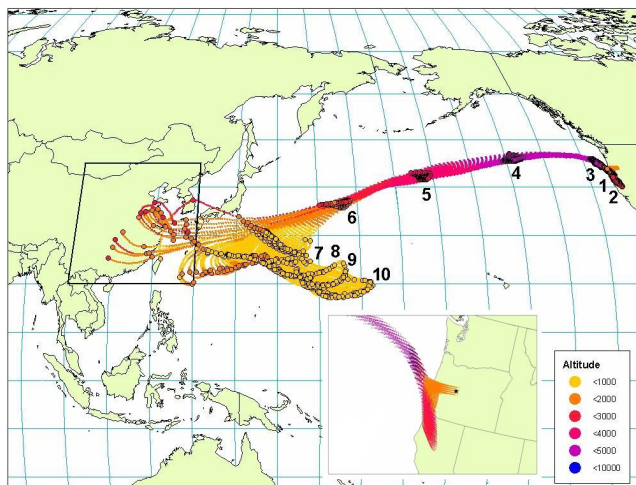


Figure 11. Back trajectory diagram with starting times of 27 April (0800–1200 UT) and a starting altitude of 1500 m AGL. A total of 125 trajectories are shown. Days 1–3 are shown in the inset figure.

of the low-altitude trajectories from days 6–10 originate over the subtropical Pacific Ocean (15–25°N) and thus these air masses are subject to considerably more photochemical aging than higher altitude, northerly air masses.

4. Conclusions

[46] Our results from this initial measurement campaign at Mount Bachelor Observatory indicate that this site at 2.8 km ASL is suitable for observing the free troposphere. On average, our measurements reflect a mixture of BL and FT air, as determined from diurnal cycles of WV and O₃ and a comparison with radiosonde data, but these periods can be effectively characterized using WV as a segregation tool. By focusing on the driest and wettest 20% of the data, we find that these represent very different types of air masses with different chemical compositions and transport histories. For example, CO, TGM, and O₃ are significantly enhanced in the dry data by 25 ppbv, 0.16 ng/m³, and 13.9 ppbv, respectively. This indicates that ALRT has a large influence during the spring at this site, and that transport at higher altitudes is more efficient than at lower altitudes. The dry data also display characteristics of recently subsided air masses from higher altitudes with colder temperatures, higher pressures, and northerly wind directions. We estimate the average altitude of the dry air masses is 3.4 km on the basis of a comparison with the WV vertical profile from Medford, Oregon.

[47] Concentrations of CO, TGM, and σ_{sp} measured at MBO are higher than those measured from a similar altitude during previous aircraft campaigns. This finding is corroborated by other CO observations, including satellite and CMDL flask observations. The difference indicates more influence from Asian sources compared to previous years, perhaps in part because of the large Siberian forest fires of 2003.

[48] Three pollution events are analyzed in detail during the spring campaign: 25 April and 13 May (ALRT) and 27 April (local). Even though the 25 April event was much larger than the 13 May event, both displayed

similar features. For example, the ratio of enhancement for each event between TGM and CO was 0.0045 – 0.0048 ng/m³/ppbv, similar to the value thought to be representative of Asian industrial pollution. Furthermore, the $\Delta\sigma_{sp}/\Delta\text{CO}$ enhancement ratio for each event was 0.47 Mm⁻¹/ppbv, which suggests little biomass burning or dust influence. Meteorologically, each event was associated with very dry air and high pressure indicating subsidence from higher altitudes. These characteristics of ALRT are in contrast to the 27 April local pollution event, which showed a strong positive correlation between WV and CO, and was associated with falling pressure and temperature. The $\Delta\text{TGM}\Delta/\text{CO}$ enhancement ratio was only 0.0013 ng/m³ for this event reflecting the lower density of mercury sources in the local region.

[49] Hysplit kinematic back trajectories were used in a retroplume approach to determine the source regions and transport pathways for these events. For each trajectory a residence time in a predefined east Asian box was calculated for different altitudes in the box. We find that large peaks in residence time occurred during the times of the observed ALRT events, and that during the local event there was almost zero trajectory residence times in the Asian source region. For both ALRT events trajectories showed how the plume descended in the FT to the altitude of MBO over time. This finding is also supported by aerosol optical thickness measurements taken in the Pacific Northwest during the same time period. The source region for the ALRT events appears to be northeastern China, Korea, and/or southern Japan about 10 days prior to arrival at MBO. Pollutants were evidently lofted to the midlatitude westerlies and transported eastward before subsiding over our region. The source region for the local event is most likely the cities of Eugene or Medford, Oregon, or Sacramento, California. However, this plume must have been diluted because of turbulence in the BL since the enhancements during this event were much smaller than for the ALRT events.

[50] Thus MBO has proven itself as a site for observing direct transport of Asian air pollution with very little influence from local emissions. Using a combination of meteorological observations, chemical and aerosol measurements and their enhancement ratios, and kinematic back trajectories, we can effectively resolve time periods of predominantly BL and FT air masses.

[51] **Acknowledgments.** The authors would like to thank Mount Bachelor Ski Area Inc., Isaac Bertschi, and Carol Higgenbotham for their assistance with field operations; Bryan Johnson for ozonesonde data; and Lyatt Jaegle for helpful discussions. We also appreciate the thoughtful comments of two anonymous reviewers. This work was supported by EPA “Science To Achieve Results (STAR)” program (R-82979701) and NSF Atmospheric Chemistry program (ATM-0425262).

References

- Akimoto, H. (2003), Global air quality and pollution, *Science*, 302, 1716–1719.
- Andreae, M. O., H. Berresheim, T. W. Andreae, M. A. Kritz, T. S. Bates, and J. T. Merrill (1988), Vertical distribution of dimethylsulfide, sulfur dioxide, aerosol ions, and radon over the northeast Pacific Ocean, *J. Atmos. Chem.*, 6, 149–173.
- Bertschi, I. T., and D. A. Jaffe (2005), Long-range transport of ozone, carbon monoxide, and aerosols to the NE Pacific troposphere during the summer of 2003: Observations of smoke plumes from Asian boreal fires, *J. Geophys. Res.*, 110, D05303, doi:10.1029/2004JD005135.

- Bertschi, I. T., D. A. Jaffe, L. Jaeglé, H. U. Price, and J. B. Dennison (2004), PHOBEA/ITCT 2002 airborne observations of transpacific transport of ozone, CO, volatile organic compounds, and aerosols to the northeast Pacific: Impacts of Asian anthropogenic and Siberian boreal fire emissions, *J. Geophys. Res.*, *109*, D23S12, doi:10.1029/2003JD004328.
- Bey, I., D. J. Jacob, J. A. Logan, and R. M. Yantosca (2001), Asian chemical outflow to the Pacific in spring: Origins, pathways, and budgets, *J. Geophys. Res.*, *106*(D19), 23,097–23,114.
- Bodhaine, B. A. (1996), Aerosol measurements during the Mauna Loa Photochemistry Experiment 2, *J. Geophys. Res.*, *101*(D9), 14,757–14,766.
- Bolton, D. (1980), The computation of equivalent potential temperature, *Mon. Weather Rev.*, *108*, 1046–1053.
- Brown, S. S., H. Stark, T. B. Ryerson, E. J. Williams, D. K. Nicks Jr., M. Trainer, F. C. Fehsenfeld, and A. R. Ravishankara (2003), Nitrogen oxides in the nocturnal boundary layer: Simultaneous in situ measurements of NO₃, N₂O₅, NO₂, NO, and O₃, *J. Geophys. Res.*, *108*(D9), 4299, doi:10.1029/2002JD002917.
- Cooper, O. R., et al. (2004a), A case study of transpacific warm conveyor belt transport: Influence of merging airstreams on trace gas import to North America, *J. Geophys. Res.*, *109*, D23S08, doi:10.1029/2003JD003624.
- Cooper, O., et al. (2004b), On the life cycle of a stratospheric intrusion and its dispersion into polluted warm conveyor belts, *J. Geophys. Res.*, *109*, D23S09, doi:10.1029/2003JD004006.
- de Gouw, J. A., et al. (2004), Chemical composition of air masses transported from Asia to the U.S. West Coast during ITCT 2K2: Fossil fuel combustion versus biomass-burning signatures, *J. Geophys. Res.*, *109*, D23S20, doi:10.1029/2003JD004202.
- Draxler, R. R., and G. D. Rolph (2003), HYSPLIT (HYbrid Single-Particle Lagrangian Integrated Trajectory) model access via NOAA ARL READY website, NOAA Air Resour. Lab., Silver Spring, Md. (Available at <http://www.arl.noaa.gov/ready/hysplit4.html>)
- Fiore, A. M., D. J. Jacob, I. Bey, R. M. Yantosca, B. D. Field, A. C. Fusco, and J. G. Wilkinson (2002), Background ozone over the United States in summer: Origin, trend, and contribution to pollution episodes, *J. Geophys. Res.*, *107*(D15), 4275, doi:10.1029/2001JD000982.
- Forster, C., et al. (2004), Lagrangian transport model forecasts and a transport climatology for the Intercontinental Transport and Chemical Transformation 2002 (ITCT 2K2) measurement campaign, *J. Geophys. Res.*, *109*, D07S92, doi:10.1029/2003JD003589.
- Friedli, H. R., L. F. Radke, R. Prescott, P. Li, J. Woo, and G. R. Carmichael (2004), Mercury in the atmosphere around Japan, Korea, and China as observed during the 2001 ACE-Asia field campaign: Measurements, distributions, sources, and implications, *J. Geophys. Res.*, *109*, D19S25, doi:10.1029/2003JD004244.
- Henne, S., M. Furger, S. Nyeki, M. Steinbacher, B. Neining, S. F. J. de Wekker, J. Dommen, N. Spichtinger, A. Stohl, and A. S. H. Prevot (2003), Quantification of topographic venting of boundary layer air to the free troposphere, *Atmos. Chem. Phys. Disc.*, *3*, 5205–5236.
- Horowitz, L. W., and D. J. Jacob (1999), Global impact of fossil fuel combustion on atmospheric NO_x, *J. Geophys. Res.*, *104*(D19), 23,823–23,840.
- Hudman, R. C., et al. (2004), Ozone production in transpacific Asian pollution plumes and implications for ozone air quality in California, *J. Geophys. Res.*, *109*, D23S10, doi:10.1029/2004JD004974.
- Jacob, D. J., J. A. Logan, and P. P. Murti (1999), Effect of rising Asian emission on surface ozone in the United States, *Geophys. Res. Lett.*, *26*, 2175–2178.
- Jaeglé, L., D. A. Jaffe, H. U. Price, P. Weiss-Penzias, P. I. Palmer, M. J. Evans, D. J. Jacob, and I. Bey (2003), Sources and budgets for CO and O₃ in the northeastern Pacific during the spring of 2001: Results from the PHOBEA-II Experiment, *J. Geophys. Res.*, *108*(D20), 8802, doi:10.1029/2002JD003121.
- Jaffe, D. A., et al. (1999), Transport of Asian air pollution to North America, *Geophys. Res. Lett.*, *26*, 711–714.
- Jaffe, D. A., I. McKendry, T. Anderson, and H. Price (2003a), Six 'new' episodes of trans-Pacific transport of air pollutants, *Atmos. Environ.*, *37*, 391–404.
- Jaffe, D., H. Price, D. Parrish, A. Goldstein, and J. Harris (2003b), Increasing background ozone during spring on the west coast of North America, *Geophys. Res. Lett.*, *30*(12), 1613, doi:10.1029/2003GL017024.
- Jaffe, D., J. Snow, and O. Cooper (2003c), The 2001 Asian dust events: Transport and impact on surface aerosol concentrations in the U.S., *Eos Trans. AGU*, *84*(46), 501.
- Jaffe, D., I. Bertschi, L. Jaeglé, P. Novelli, J. S. Reid, H. Tanimoto, R. Vingarzan, and D. L. Westphal (2004), Long-range transport of Siberian biomass burning emissions and impact on surface ozone in western North America, *Geophys. Res. Lett.*, *31*, L16106, doi:10.1029/2004GL020093.
- Jaffe, D., E. Prestbo, P. Swartzendruber, P. Weiss-Penzias, S. Kato, A. Takami, S. Hatakeyama, and Y. Kajii (2005), Export of atmospheric mercury from Asia, *Atmos. Environ.*, *39*, 3029–3038.
- Kellerhals, M., S. Beauchamp, W. Belzer, P. Blanchard, F. Froude, and B. Harvey (2003), Temporal and spatial variability of total gaseous mercury in Canada: Results from the Canadian Atmospheric Mercury Measurement Network (CAMNet), *Atmos. Environ.*, *37*, 1003–1011.
- Kotchenruther, R. A., D. A. Jaffe, H. J. Beine, T. L. Anderson, J. W. Bottenheim, J. M. Harris, D. R. Blake, and R. Schmitt (2001), Observations of ozone and related species in the northeast Pacific during the PHOBEA campaigns: 2. Airborne observations, *J. Geophys. Res.*, *103*, 7463–7483.
- Lee, D. S., G. J. Dollard, and S. Pepler (1998), Gas-phase mercury in the atmosphere of the United Kingdom, *Atmos. Environ.*, *32*, 855–864.
- Liang, Q., L. Jaeglé, D. A. Jaffe, P. Weiss-Penzias, A. Heckman, and J. A. Snow (2004), Long-range transport of Asian pollution to the northeast Pacific: Seasonal variations and transport pathways of carbon monoxide, *J. Geophys. Res.*, *109*, D23S07, doi:10.1029/2003JD004402.
- Lin, C., and S. O. Pehkonen (1999), The chemistry of atmospheric mercury: A review, *Atmos. Environ.*, *33*, 2067–2079.
- Liu, H., D. J. Jacob, I. Bey, R. M. Yantosca, B. N. Duncan, and G. W. Sachse (2003), Transport pathways for Asian pollution outflow over the Pacific: Interannual and seasonal variations, *J. Geophys. Res.*, *108*(D20), 8786, doi:10.1029/2002JD003102.
- Logan, J. A. (1999), An analysis of ozonesonde data for the troposphere: Recommendations for testing 3-D models and development of a gridded climatology for tropospheric ozone, *J. Geophys. Res.*, *104*(D13), 16,115–16,150.
- Novelli, P. C., J. E. Elkins, and L. P. Steele (1991), The development and evaluation of a gravimetric reference scale for measurements of atmospheric carbon monoxide, *J. Geophys. Res.*, *96*, 13,109–13,121.
- Nowak, J. B., et al. (2004), Gas-phase chemical characteristics of Asian emission plumes observed during ITCT 2K2 over the eastern North Pacific Ocean, *J. Geophys. Res.*, *109*, D23S19, doi:10.1029/2003JD004488.
- Oltmans, S. J., et al. (2004), Tropospheric ozone over the North Pacific from ozonesonde observations, *J. Geophys. Res.*, *109*, D15S01, doi:10.1029/2003JD003466.
- Oshima, N., et al. (2004), Asian chemical outflow to the Pacific in late spring observed during the PEACE-B aircraft mission, *J. Geophys. Res.*, *109*, D23S05, doi:10.1029/2004JD004976.
- Pacyna, E. G., and J. M. Pacyna (2002), Global emission of mercury from anthropogenic sources in 1995, *Water Air Soil Pollut.*, *137*, 149–165.
- Parrish, D. D., C. J. Hahn, E. J. Williams, R. B. Norton, F. C. Fehsenfeld, H. B. Singh, J. D. Shetter, B. W. Gandrud, and B. A. Ridley (1992), Indication of photochemical histories of Pacific air masses from measurements of atmospheric trace species at Point Arena, California, *J. Geophys. Res.*, *97*, 15,883–15,901.
- Parrish, D. D., Y. Kondo, O. R. Cooper, C. A. Brock, D. A. Jaffe, M. Trainer, T. Ogawa, G. Hübler, and F. C. Fehsenfeld (2004a), Intercontinental Transport and Chemical Transformation 2002 (ITCT 2K2) and Pacific Exploration of Asian Continental Emission (PEACE) experiments: An overview of the 2002 winter and spring intensives, *J. Geophys. Res.*, *109*, D23S01, doi:10.1029/2004JD004980.
- Parrish, D. D., et al. (2004b), Changes in the photochemical environment of the temperate North Pacific troposphere in response to increased Asian emissions, *J. Geophys. Res.*, *109*, D23S18, doi:10.1029/2004JD004978.
- Poissant, L., M. Pilote, X. Xu, H. Zhang, and C. Beauvais (2004), Atmospheric mercury speciation and deposition in the Bay St. François wetlands, *J. Geophys. Res.*, *109*, D11301, doi:10.1029/2003JD004364.
- Price, H. U., D. A. Jaffe, P. V. Doskey, I. McKendry, and T. Anderson (2003), Vertical profiles of O₃, aerosols, CO and NMHCs in the Northeast Pacific during the TRACE-P and ACE-ASIA experiments, *J. Geophys. Res.*, *108*(D20), 8799, doi:10.1029/2002JD002930.
- Price, H. U., D. A. Jaffe, O. R. Cooper, and P. V. Doskey (2004), Photochemistry, ozone production, and dilution during long-range transport episodes from Eurasia to the northwest United States, *J. Geophys. Res.*, *109*, D23S13, doi:10.1029/2003JD004400.
- Schroeder, W. H., and J. Munthie (1998), Atmospheric mercury—An overview, *Atmos. Environ.*, *32*, 809–822.
- Shindell, D. T., G. Faluvegi, and L. K. Emmons (2005), Inferring carbon monoxide pollution changes from space-based observations, *J. Geophys. Res.*, *110*, D23303, doi:10.1029/2005JD006132.
- Stohl, A. (1998), Computation, accuracy and applications of trajectories—A review and bibliography, *Atmos. Environ.*, *32*, 947–966.
- Stohl, A., S. Eckhardt, C. Forster, P. James, N. Spichtinger, and P. Seibert (2002), A replacement for simple back trajectory calculation in the interpretation of atmospheric trace substance measurements, *Atmos. Environ.*, *36*, 4635–4648.

- Stohl, A., C. Forster, S. Eckhardt, N. Spichtinger, H. Huntrieser, J. Heland, H. Schlager, S. Wilhelm, F. Arnold, and O. Cooper (2003), A backward modeling study of intercontinental pollution transport using aircraft measurements, *J. Geophys. Res.*, *108*(D12), 4370, doi:10.1029/2002JD002862.
- Streets, D. G., et al. (2003), An inventory of gaseous and primary aerosol emissions in Asia in the year 2000, *J. Geophys. Res.*, *108*(D21), 8809, doi:10.1029/2002JD003093.
- Suntharalingam, P., D. J. Jacob, P. I. Palmer, J. A. Logan, R. M. Yantosca, Y. Xiao, M. J. Evans, D. G. Streets, S. L. Vay, and G. W. Sachse (2004), Improved quantification of Chinese carbon fluxes using CO₂/CO correlations in Asian outflow, *J. Geophys. Res.*, *109*, D18S18, doi:10.1029/2003JD004362.
- Wang, Q., W. Shen, and Z. Ma (2000), Estimation of mercury emission from coal combustion in China, *Environ. Sci. Technol.*, *34*, 2711–2713.
- Weingartner, E., S. Nyeki, and U. Baltensperger (1999), Seasonal and diurnal variation of aerosol size distributions ($10 < D < 750$ nm) at a high-alpine site (Jungfraujoch 3580 m asl), *J. Geophys. Res.*, *104*(D21), 26,809–26,820.
- Weiss-Penzias, P., D. A. Jaffe, A. McClintick, E. M. Prestbo, and M. S. Landis (2003), Gaseous elemental mercury in the marine boundary layer: Evidence for rapid removal in anthropogenic pollution, *Environ. Sci. Technol.*, *37*, 3755–3763.
- Weiss-Penzias, P., D. A. Jaffe, L. Jaeglé, and Q. Liang (2004), Influence of long-range-transported pollution on the annual and diurnal cycles of carbon monoxide and ozone at Cheeka Peak Observatory, *J. Geophys. Res.*, *109*, D23S14, doi:10.1029/2004JD004505.
- Yienger, J. J., II (2000), The episodic nature of air pollution transport from Asia to North America, *J. Geophys. Res.*, *105*(D22), 26,931–26,946.
-
- D. Chand, W. Hafner, D. A. Jaffe, P. Swartzendruber, and P. Weiss-Penzias, Interdisciplinary Arts and Sciences Department, University of Washington, Bothell, WA 98011, USA. (pweiss@bothell.washington.edu)
- J. B. Dennison, Washington State Department of Ecology, P.O. Box 47600, Olympia, WA 98504, USA.
- E. Prestbo, Frontier Geosciences, 414 Pontius Avenue N, Seattle, WA 98109, USA.